electronic reprint

Journal of
Applied Crystallography
ISSN 0021-8898

Diffraction peak profiles from spherical crystallites with lognormal size distribution

T. Ida, S. Shimazaki, H. Hibino and H. Toraya

Journal of
Applied Crystallography
ISSN 0021-8898

Received 24 December 2002
Accepted 27 May 2003

Diffraction peak profiles from spherical crystallites with lognormal size distribution

T. Ida,* S. Shimazaki, H. Hibino and H. Toraya

Ceramics Research Laboratory, Nagoya Institute of Technology, Asahigaoka, Tajimi, Gifu 507-0071, Japan. Correspondence e-mail: ida@crl.nitech.ac.jp

An efficient and accurate method to evaluate the theoretical diffraction peak profiles from spherical crystallites with lognormal size distribution (SLN profile) is presented. Precise results can be obtained typically by an eight-term numerical integral for any values of the parameters, by applying an appropriate substitution of the variable to the integral formula. The calculated SLN profiles have been verified by comparison with those calculated by inverse Fourier transform from the exact analytical solution of the Fourier-transformed SLN profile. It has been found that the shape of the SLN profile strongly depends on the variance of size distribution. When the logarithmic standard deviation ω of the size distribution is close to 0.76, the SLN profile becomes close to a Lorentzian profile, and 'super-Lorentzian' profiles are predicted for larger values of ω, as has been concluded by Popa & Balzar [*J. Appl. Cryst.* (2002), **35**, 338–346]. The intrinsic diffraction peak profiles of an SiC powder sample obtained by deconvolution of the instrumental function have certainly shown 'super-Lorentzian' line profiles, and they are well reproduced by the SLN profile for the value $\omega = 0.93$.

1. Introduction

Many important physical properties of solid materials depend on their microstructure, among which crystallite size and microstrain are the most important characteristics. In principle, these can be determined from the line profile analysis of powder X-ray diffraction data.

Since experimental diffraction peak profiles are broadened by crystallite size, lattice defects and instrumental aberrations, it is essential to separate these effects correctly. Three classical methods, namely (i) the Stokes (1948) method for eliminating instrumental aberrations, and (ii) the Warren–Averbach (1950) and (iii) the Williamson–Hall (1952) methods for separating size and strain effects, have been used during the past five decades.

The Stokes (1948) method is based on the deconvolution of the instrumental function by a Fourier method. The experimental line profiles of a standard sample, which should be prepared by long-time annealing at sufficiently high temperatures, are used as instrumental functions in the Stokes method.

The Warren–Averbach (1950) and Williamson–Hall (1952) methods separate the size and strain effects by their different dependence on the diffraction vector k. The former is based on the Fourier coefficients of the line profiles, while the latter is based on the widths of the line profiles.

In this paper, we focus our attention on the effects of crystallite size distribution on powder diffraction data. It is known that the area-weighted average size $\langle D\rangle_A$ is estimated from the initial slope of the Fourier transform in the Warren–Averbach analysis, while the volume-weighted average size $\langle D\rangle_V$ is estimated by the Williamson–Hall method when it is applied to the intrinsic integral breadths of the line profiles (Guinier, 1963). It has been observed by many authors that the size distribution of crystallites in a powder or polycrystalline solid is lognormal (*cf.* Langford *et al.*, 2000). By assuming the lognormal size distribution, the mean size and the variance, which determine all the characteristics of the lognormal distribution, can be estimated from the two different values of $\langle D\rangle_A$ and $\langle D\rangle_V$.

Recently, significant improvements in diffraction line profile analysis, which are particularly useful in the evaluation of crystallite size distribution, have been achieved by Langford *et al.* (2000), Ungár *et al.* (2001) and Ida & Toraya (2002).

Langford *et al.* (2000) have shown that the size distribution can be determined directly by a profile fitting method, applying the theoretical diffraction line profile from spherical crystallites with lognormal size distribution (hereafter abbreviated as the 'SLN profile'). In principle, the SLN profile as an integral formula can be evaluated numerically. The integral breadth and the Fourier initial slope can simultaneously be evaluated for each diffraction peak by a simple profile fitting procedure applying the SLN profile function. When the size effect is dominant in an observed line profile, the size distribution can be determined straightforwardly. However, their evaluation and the application of the SLN profile have been restricted to a small variance of the distribution (Popa & Balzar, 2002).

Ungár *et al.* (2001) have shown that the exact solution of the Fourier transform of the SLN profile is available in closed form. They have applied the formula to fit the Fourier-transformed experimental peak profiles of fine silicon nitride powder. Both the Fourier initial slopes and the integral breadths have been evaluated by fitting to the Fourier-transformed line profiles, similarly to the method of Langford *et al.* (2000). It has been reported that the size distribution determined by the fitting method is in good agreement with the results of transmission electron microscopy (TEM).

We have recently developed a new technique to eliminate the instrumental aberrations from the experimental diffraction data (Ida & Toraya, 2002). Since the method is based on analytical expressions for the instrumental aberrations (Ida, 1998*a*; Ida & Kimura, 1999*a*,*b*), no measurement of standard samples is required, and the whole diffraction pattern can simultaneously be treated no matter how complicated the pattern may be. Estimation of the errors in the deconvoluted data have also been enabled. The method would be particularly useful in the estimation of size distribution by fitting the SLN profile to experimental peak profiles of relatively large crystallites, where the effects of instrumental aberrations are not negligible.

In this paper, we present an efficient algorithm to evaluate theoretical SLN profiles in high precision for any values of the logarithmic standard deviation ω. The calculated line profiles are verified by comparison with the inverse Fourier transform of the exact analytical solution of the Fourier-transformed line profile given by Ungár *et al.* (2001). The possibility of a Lorentzian or a 'super-Lorentzian' size effect for lognormal distribution is theoretically examined. Although Langford *et al.* (2000) have concluded that a Lorentzian or 'super-Lorentzian' size effect might be attributed to a non-unimodal size distribution, it seems that their results also suggest that the line profiles of lognormal size distribution can be Lorentzian or become 'super-Lorentzian' in shape for large values of the logarithmic standard deviation ω. The intrinsic diffraction peak profiles of an SiC powder sample, obtained by the whole-pattern deconvolution method, are analysed by applying the SLN profile model. The results are compared with the experimental results of laser diffraction, scanning electron microscopy (SEM), and the specific surface area measured by the Brunauer–Emmett–Teller (BET) method.

2. Theory

2.1. Line profiles

According to Langford & Wilson (1978), the diffraction peak intensity profile for the diffraction vector $k = 2(\sin\theta - \sin\theta_{\rm Bragg})/\lambda$ from a spherical crystallite is given by

$$I_S(k; D) = (\pi D^4/2)s^{-2}[1 - 2s^{-1}\sin s + 4s^{-2}\sin^2(s/2)], \quad (1)$$

where D is the diameter and $s = 2\pi kD$. The normalized formula for the peak profile function $f_S(k; D)$ is derived from the normalized Fourier formula for a spherical crystallite:

$$A_S(L; D) = 1 - 3|L|/2D + |L|^3/2D^3, \quad (2)$$

which gives

$$f_S(k; D) = \int_{-D}^{D} A_S(L; D)\exp(-2\pi ikL)\,{\rm d}L = 3Ds^{-2}[1 - 2s^{-1}\sin s + 4s^{-2}\sin^2(s/2)]. \quad (3)$$

It should be noted that the following relations,

$$I_S(k; D) = (\pi D^3/6)f_S(k; D) \quad (4)$$

and

$$f_S(k; D) \rightarrow 3D/4 (k \rightarrow 0), \quad (5)$$

are readily derived from the above equations.

It is assumed that the crystallite size obeys lognormal distribution with the median m and logarithmic standard deviation ω, the density function of which is given by

$$f_{\rm LN}(D; m, \omega) = [D\omega(2\pi)^{1/2}]^{-1}\exp\{-[\ln(D/m)]^2/2\omega^2\}, \quad (6)$$

and the cumulative distribution function is

$$F_{\rm LN}(D; m, \omega) = (1/2){\rm erfc}[-\ln(D/m)/2^{1/2}\omega], \quad (7)$$

where the function erfc(x) is the complementary error function defined by

$${\rm erfc}(x) \equiv (2/\pi^{1/2})\int_x^\infty \exp(-t^2)\,{\rm d}t. \quad (8)$$

The properties of the lognormal distribution have been briefly reviewed by Langford *et al.* (2000). The jth moment of the distribution is given by

$$\langle D^j\rangle \equiv \int_0^\infty D^j f_{LN}(D; m, \omega)\,{\rm d}D = m^j\exp(j^2\omega^2/2), \quad (9)$$

from which the arithmetic mean is

$$\langle D\rangle = m\exp(0.5\omega^2), \quad (10)$$

the variance is

$$\sigma^2 = \langle D\rangle^2[\exp(\omega^2) - 1], \quad (11)$$

the area-weighted mean is

$$\langle D\rangle_A = \langle D^3\rangle/\langle D^2\rangle = m\exp(2.5\omega^2), \quad (12)$$

and the volume-weighted mean is

$$\langle D\rangle_V = \langle D^4\rangle/\langle D^3\rangle = m\exp(3.5\omega^2). \quad (13)$$

The diffraction peak intensity profile from lognormally distributed spherical particles is given by

$$I_{\rm SLN}(k; m, \omega) = \int_0^\infty I_S(k; D)f_{\rm LN}(D; m, \omega)\,{\rm d}D, \quad (14)$$

while the normalized formula is given by

$$f_{\rm SLN}(k; m, \omega) = \int_0^\infty f_S(k; D)f_{\rm LN}[D; m\exp(3\omega^2), \omega]\,{\rm d}D. \quad (15)$$

From equations (5) and (9), the peak top value of $f_{\rm SLN}(k; m, \omega)$ is given by

$$f_{\rm SLN}(k; m, \omega) \rightarrow (3m/4)\exp(3.5\omega^2) \qquad (k \rightarrow 0), \tag{16}$$

and the integral breadth is

$$\beta_{\rm SLN} = (4/3)\langle D\rangle_V^{-1} = (4/3m)\exp(-3.5\omega^2). \tag{17}$$

2.2. Fourier-transformed line profile

Although it is difficult to solve the integral in equation (15) analytically, the exact solution of the Fourier transform

$$A_{\rm SLN}(L; m, \omega) \equiv \int_{-\infty}^{\infty} f_{\rm SLN}(k; m, \omega)\exp(2\pi ikL)\,{\rm d}k \tag{18}$$

is available (Ungár *et al.*, 2001). The solution is

$$\begin{aligned} A_{\rm SLN}(L; m, \omega) &= (1/2){\rm erfc}\{[\ln(|L|/m) - 3\omega^2]/2^{1/2}\omega\} \\ &\quad - (3|L|/4m)\exp(-2.5\omega^2){\rm erfc}\{[\ln(|L|/m) - 2\omega^2]/2^{1/2}\omega\} \\ &\quad + (|L|^3/4m^3)\exp(-4.5\omega^2){\rm erfc}\{[\ln(|L|/m)]/2^{1/2}\omega\}. \end{aligned} \tag{19}$$

The initial slope of the Fourier transform is then given by

$$\begin{aligned} (\partial A_{\rm SLN}/\partial L) &\rightarrow \mp(3/2m)\exp(-2.5\omega^2) \\ &= \mp(3/2)\langle D\rangle_A^{-1} \quad (L \rightarrow \pm 0) \end{aligned} \tag{20}$$

Fig. 1 shows the Fourier transforms $A_{\rm SLN}(L; m, \omega)$ calculated by equation (19) for the common value of $\langle D\rangle_V = 1$ on variation of the logarithmic standard deviation ω.

2.3. Evaluation of the line profile

Even though the SLN prolile is clearly defined by equation (15) in integral form, it is not easy to evaluate the integral numerically, especially for large values of ω. Langford *et al.* (2000) have presented the formula

$$f_{\rm SLN}(k; m, \omega) = \int_0^{\infty} I_S(k; D)\,{\rm d}\Lambda \Big/ \int_0^{\infty} (\pi D^3/6)\,{\rm d}\Lambda, \tag{21}$$

where

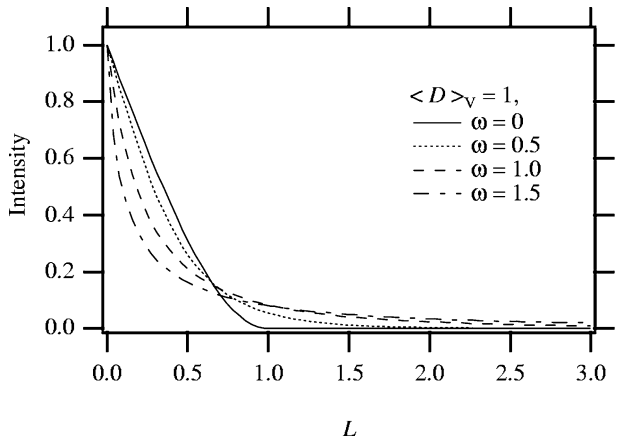

Figure 1
The Fourier transforms of the SLN profiles for the median $m = \exp(-3.5\omega^2)$ ($\langle D\rangle_V = 1$) and the logarithmic standard deviation $\omega = 0$, 0.5, 1, 1.5.

$$\Lambda \equiv F_{\rm LN}(D; m, \omega). \tag{22}$$

Alternatively, Popa & Balzar (2002) have proposed the numerical formulae

$$f_{\rm SLN}(k; m, \omega) \simeq m\exp(3.5\omega^2)\sum_{j=1}^{N} w_j fs(k; D_j)/D_j \tag{23}$$

and

$$D_j = m\exp(4\omega^2 + 2^{1/2}\omega y_j), \tag{24}$$

where $\{y_j\}$ and $\{w_j\}$ are the abscissas and weights for the N-term Gauss–Hermite quadrature. The above formula gives the exact peak value for a normalized set of weights $\{w_j\}$, *i.e.* $\sum_j w_j = 1$. Popa & Balzar (2002) have treated the profiles calculated by a 16-term Gauss–Hermite quadrature on equation (23) as the 'exact' profile for the range $0 \leq \omega \leq 1.39$. However, application of such formulae given by equations (23) and (24) is only valid for small values of ω, which correspond to a slight modification from $f_S(k; m)$. For large ω, the calculated profiles would be considerably deviated from the exact solution and the accuracy would only be improved slowly by increasing the number of terms N. Fig. 2 show how the results calculated by equations (23) and (24) change on the increasing N, for the case $\omega = (\ln 7)^{1/2}$. The SLN profile calculated by a 65536-point inverse Fourier transform of the exact Fourier-transformed profile given by equation (19) with a step size of 1/409.6 on the L scale is also shown as markers in Fig. 2.

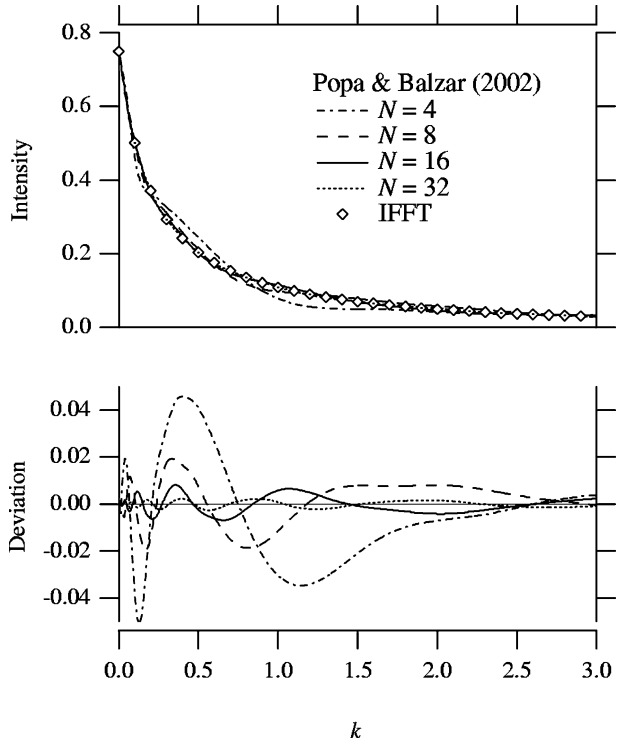

Figure 2
Evaluation of the SLN profile for $m = \exp(-3.5\omega^2)$ ($\langle D\rangle_V = 1$) and $\omega = (\ln 7)^{1/2} = 1.39496$ on increasing the number of terms N, applying equations (23) and (24) proposed by Popa & Balzar (2002). The open diamonds mark the values obtained by the inverse Fourier transform of the exact Fourier-transformed profile.

Table 1
The abscissas x_j and weights w_j for eight-term (N = 8) Gauss–Legendre quadrature.

For $j \geq 5$, use the following relations: $x_{N+1-j} = 1 - x_j$; $w_{N+1-j} = w_j$.

	j = 1	j = 2	j = 3	j = 4
x_j	0.01985507	0.10166676	0.23723380	0.40828268
w_j	0.05061427	0.11119052	0.15685332	0.18134189

The results given in Fig. 2 by the method proposed by Popa & Balzar (2002) are found to be considerably deviated from the profile calcuclated by the inverse Fourier transform of the exact analytical solution. The maximum deviation of the results of the 16-term numerical integral exceeds 1.08% relative to the peak height, the amount of which cannot be neglected in the application to profile fitting analysis.

As one of the authors has already reported (Ida & Kimura, 1999*a*,*b*), convolution of peak profile functions can be properly evaluated by applying formulae derived from an appropriate substitution of the variable. The method is also applicable to the evaluation of the SLN function $f_{\rm SLN}(k; m, \omega)$ with only slight modification, which gives the following formulae:

$$f_{\rm SLN}(k; m, \omega) \simeq H_0 \sum_{j=1}^{N} w_j g_j / G'_j, \tag{25}$$

$$D_0 = m \exp(4\omega^2), \tag{26}$$

$$G_0 = (\pi k)^{-1} \arctan(3\pi k D_0/2), \tag{27}$$

$$H_0 = 2^{-1} \exp(-0.5\omega^2) G_0, \tag{28}$$

$$\xi_j = x_j G_0, \tag{29}$$

$$D'_j = (4/3\pi k) \tan(\pi k \xi_j), \tag{30}$$

$$D_j = m \exp[4\omega^2 - 2^{1/2}\omega \,\mathrm{erfc}^{-1}(D'_j/D_0)], \tag{31}$$

$$g_j = f_S(k; D_j)/D_j, \tag{32}$$

$$G'_j = (3/4)[1 + (3\pi k D'_j/4)^2]^{-1}, \tag{33}$$

$$(j = 1, \ldots, N)$$

where $\{x_j\}$ and $\{w_j\}$ are the abscissas and weights of the Gauss–Legendre quadrature (Press *et al.*, 1986). The details of the derivation are described in Appendix *A*. A numerical routine for evaluating the inverse complementary error function $\mathrm{erfc}^{-1}(x)$ is given in Appendix *B*.

Fig. 3 shows the results of the calculation by the formulae given by equations (25)–(33) for $\omega = (\ln 7)^{1/2} = 1.39496$, on increasing the number of terms N up to 16. Interestingly, even the two-term numerical integral (N = 2) gives values considerably close to those calculated by the inverse Fourier transform of $A_{\rm SLN}(L; m, \omega)$, and the numerical integral rapidly approaches the expected value on increasing N. The deviation of our eight-term numerical integral is within 0.32% relative to the peak height.

Table 1 lists the abscissas $\{x_j\}$ and weights $\{w_j\}$ for the eight-term (N = 8) Gauss–Legendre integral, created by a routine `gauleg()` given by Press *et al.* (1986). The SLN profiles for ω = 0, 0.5, 1, 1.5, calculated by the eight-term numerical integrals, are shown in Fig. 4. All of the calculated profiles coincided well with those derived from the inverse Fourier transform of $A_{\rm SLN}(L; m, \omega)$ calculated by equation (19).

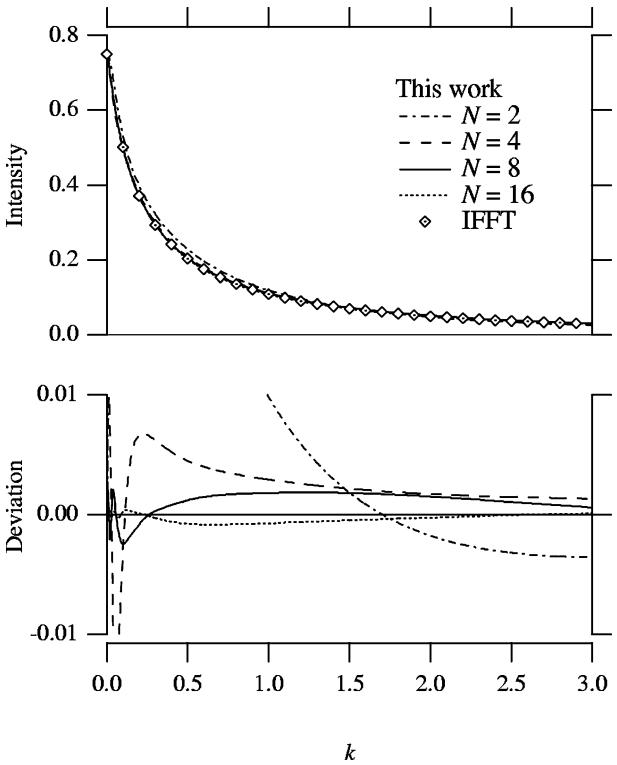

Figure 3
Evaluation of the SLN profile for $m = \exp(-3.5\omega^2)$ ($\langle D \rangle_V = 1$) and $\omega = (\ln 7)^{1/2} = 1.39496$ on increasing the number of terms N, applying equations (30) and (31). The open diamonds mark the values obtained by the inverse Fourier transform of the exact Fourier-transformed profile.

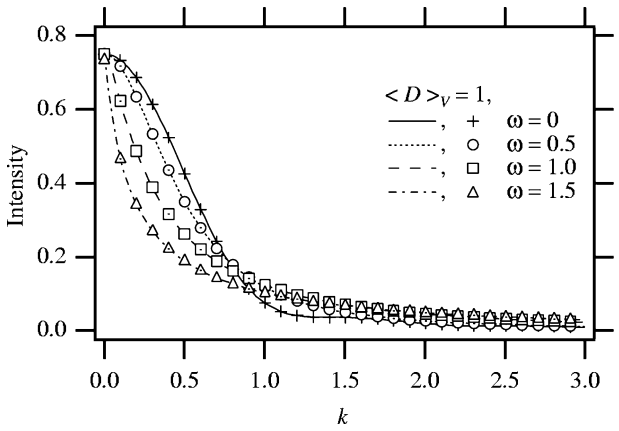

Figure 4
The SLN profiles for the median $m = \exp(-3.5\omega^2)$ ($\langle D \rangle_V = 1$) and the logarithmic standard deviation ω = 0, 0.5, 1, 1.5. Markers denote the values obtained by the inverse Fourier transform of the Fourier-transformed profile.

2.4. Comparison with the Lorentzian profile

Although Langford *et al.* (2000) have suggested that the Lorentzian or 'super-Lorentzian' size effect might be attributed to a non-unimodal size distribution, it seems that both shapes can be rather naturally explained by the unimodal lognormal size distribution with large logarithmic standard deviation ω, as has been concluded by Popa & Balzar (2002).

The Lorentzian profile with the full width at half-maximum (FWHM) of 2γ is given by

$$f_L(k;\gamma) = (\pi\gamma)^{-1}[1 + (k/\gamma)^2]^{-1}, \tag{34}$$

and the Fourier transform is

$$A_L(L;\gamma) = \exp(-2\pi\gamma|L|). \tag{35}$$

The integral breadth is then $\pi\gamma$ and the initial slope of the Fourier coefficient is $|(\partial A_L/\partial L)_0| = 2\pi\gamma$. Those properties are exactly the same as the SLN profile with $m = (3/4)^6/\pi\gamma$ and $\omega = [\ln(16/9)]^{1/2} = 0.758528$.

Fig. 5 shows both the Lorentzian profile and the SLN profile with $\omega = [\ln(16/9)]^{1/2}$. The close resemblance clearly indicates that the line profiles of crystallites with lognormal size distribution can certainly become a 'Lorentzian-like' profile for a realistic value of $\omega \simeq 0.76$, even though it would be intermediate between Lorentzian and Gaussian for a narrower distribution of size (Langford *et al.*, 2000). Furthermore, 'super-Lorentzian' (Wertheim *et al.*, 1974) line profiles, which have sometimes been reported (*e.g.* Plévert & Louër, 1990), are also likely to be observed in the case of a broader size distribution.

3. Application to an SiC powder sample

3.1. Experimental

A commercial SiC powder sample (JFCC, RP-2) was used for the experiments. The cumulative size distribution measured with a laser diffraction instrument (Malvern, MasterSizer) and the optimized lognormal distribution are shown in Fig. 6. The optimized values of the parameters for the distribution are $\langle D\rangle_V \simeq 600$ nm and $\omega = 0.97$ (3).

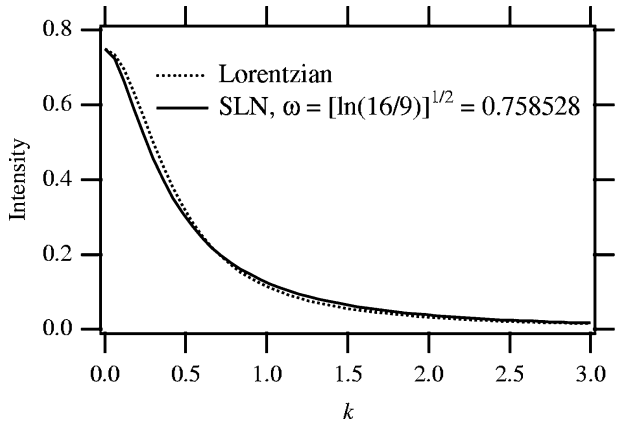

Figure 5
Comparison between the Lorentzian (dotted) and SLN (solid) line profiles.

Fig. 7 shows the scanning electron micrograph (SEM) of the powder. Although it is difficult to estimate the size distribution from the SEM photograph, the apparent particle size is found to be widely distributed, ranging from 50 to 1000 nm.

The specific surface of the powder, measured by the method of Brunauer–Emmett–Teller (BET), was 22.93 $m^2\ g^{-1}$, from which the area-weighted average size was estimated as $\langle D\rangle_A = 80.9$ nm.

The powder diffraction pattern was measured with a conventional powder X-ray diffractometer (Rigaku, RAD2C) with a Cu $K\alpha$ radiation tube operated as a line focus at 40 kV and 30 mA, and with a curved graphite monochromator on the diffracted-beam side. The radius of the goniometer circle was $R = 250$ mm; a receiving sit of 0.15 mm width, and 1° open divergence and scattering slits were used. The axial divergence was limited to $\Phi_A = 2.5°$ in FWHM by symmetrically located sets of Soller slits. The SiC powder was loaded into the hollow [0.553 (7) mm depth] of a glass holder with the filling factor of 35.8 (4). The penetration depth of the Cu $K\alpha$ X-ray was estimated at 0.199 (2) mm, which was sufficiently shorter than the thickness of the sample. The pattern was scanned over the angular range 33–125° (2θ), with a step length of 0.05° (2θ) and a counting time of 40 s per step.

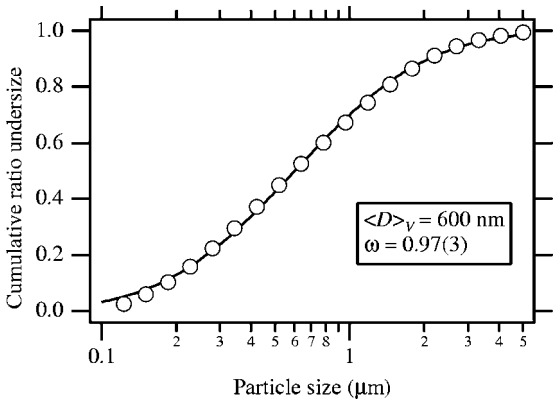

Figure 6
Particle size distribution of SiC powder measured with a laser diffraction instrument. Open circles denote the observed values and the line shows the optimized lognormal distribution.

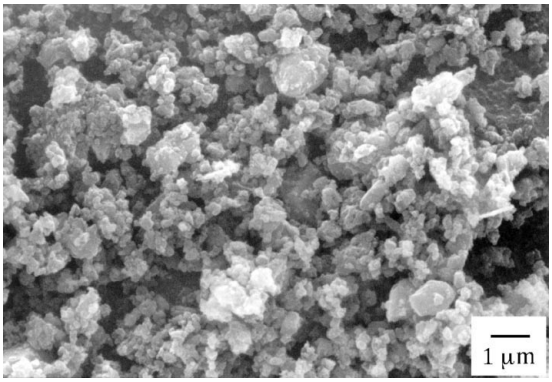

Figure 7
SEM micrograph of an SiC powder sample.

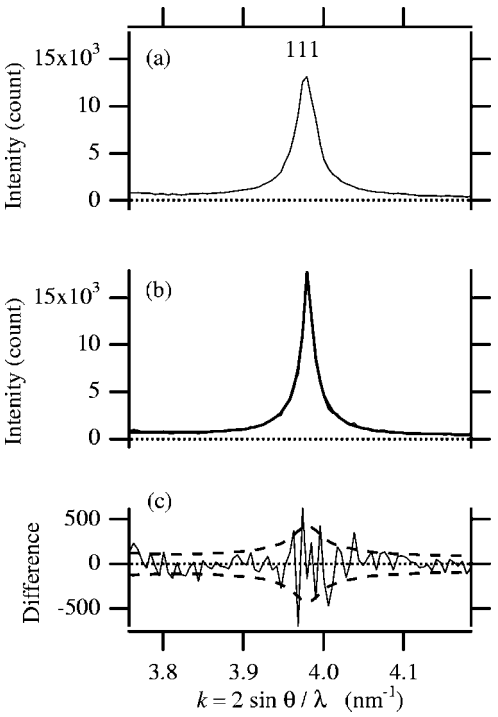

Figure 8
The 111 diffraction peak profiles of an SiC powder sample: (*a*) raw experimental data, (*b*) deconvoluted data (thin line) and the optimized SLN profile (thick line), (*c*) the difference plot (solid line) and the estimated error (broken lines).

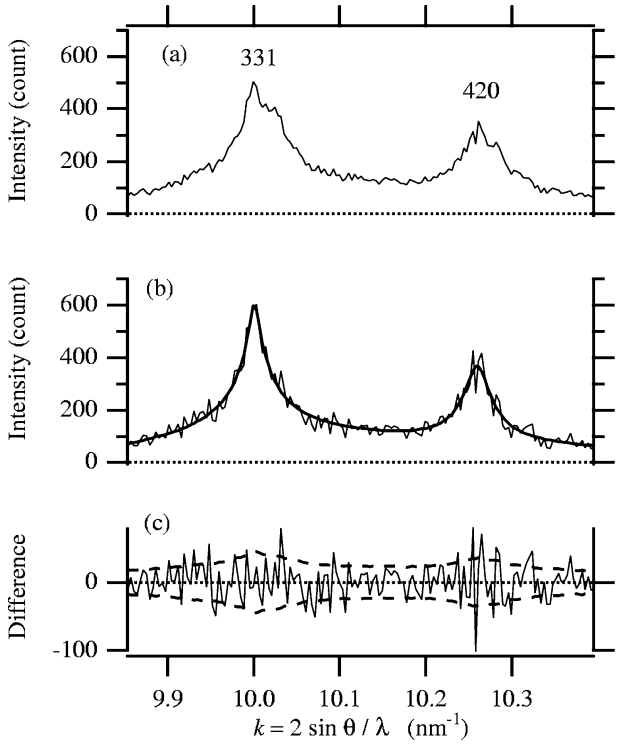

Figure 9
The 331 and 420 diffraction peak profiles of an SiC powder sample: (*a*) raw experimental data, (*b*) deconvoluted data (thin line) and the optimized SLN profile (thick line), (*c*) the difference plot (solid line) and the estimated error (broken lines).

3.2. Elimination of instrumental aberrations

The $K\alpha_2$ sub-peak and instrumental aberrations caused by the axial divergence, flat-specimen and sample transparency were removed from the experimental data by the whole-pattern deconvolution method recently developed by the authors (Ida & Toraya, 2002). The effects of the finite widths of the X-ray source and receiving slit were also deconvoluted, assuming the effective width of the X-ray source to be 0.1 mm. The smoothing filter was not applied for simplicity in the estimation of the profile parameters. The errors in the deconvoluted data were evaluated by the correlation of the reciprocal variance in the source data and the squared instrumental function.

Figs. 8(*a*) and 9(*a*) show the raw diffraction data around the 111, 331 and 420 reflections of the SiC powder, while Figs. 8(*b*) and 9(*b*) show the deconvoluted profiles. The deconvoluted profiles have symmetric shape, sharpened peak-tops and also significantly long tails, which are the characteristic features of a so-called 'super-Lorentzian' profile (Wertheim *et al.*, 1974).

3.3. Profile fitting

The deconvoluted profiles were individually fitted with the SLN peak profile function $f_{\rm SLN}(k; m, \omega)$, calculated by the efficient algorithm based on the eight-term numerical integral. A combination of two profile functions was used for two pairs of reflections, (311 and 222) and (331 and 422). A quadratic background was assumed for each analysed data range. Both the median diameter m and the logarithmic standard deviation ω were treated as adjustable parameters.

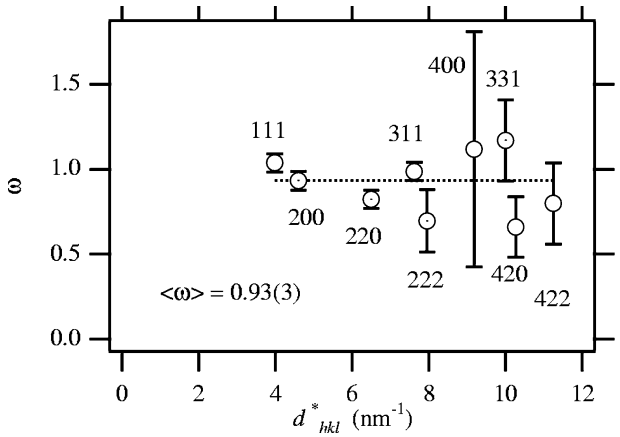

Figure 10
The optimized values of the logarithmic standard deviation ω of the SLN profiles for 111–422 reflections.

The results of profile fitting for the 111, 331 and 420 reflections are shown in Figs. 8(*b*), 8(*c*), 9(*b*) and 9(*c*). As seen in Figs. 8(*b*) and 9(*b*), the SLN profiles fit the deconvoluted data very well. No significant systematic deviation is found in the difference plots in Figs. 8(*c*) and 9(*c*).

3.4. Line profile analysis

The optimized values of the logarithmic standard deviation ω for the 111–422 reflections are shown in Fig. 10. The

weighted average has been estimated at $\langle\omega\rangle$ = 0.93 (3), which is close to the value of 0.97 (3) evaluated by the laser diffraction method. The observed 'super-Lorentzian' profiles are naturally ascribed to the broad size distribution.

The integral breadth calculated by $\beta_{\rm SLN} = (4/3m)\exp(-3.5\omega^2)$ for each reflection is plotted *versus* d^*_{hkl} in Fig. 11, which is identical to the Williamson–Hall plot (Williamson & Hall, 1953). The optimized linear dependence is given by

$$\beta_{\rm SLN} = 0.024\ (4)\ {\rm nm}^{-1} + 0.0040\ (6)\ d^*_{hkl}.$$

The volume-weighted average size of crystallites is formally estimated at 50–70 nm, which appears to be considerably smaller than the particle size observed in laser diffraction and BET experiments. It has been suggested that the coherently diffracting domain of the SiC sample is smaller than the apparent particle size. It should be noted that the line widths might be affected by the line broadening caused by stacking faults, which may arise in the SiC crystallites (Paterson, 1952).

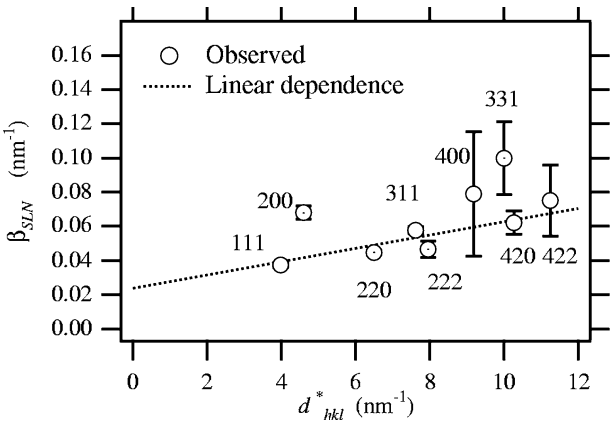

Figure 11
The integral breadth $\beta_{\rm SLN}$ plotted *versus* the reciprocal interplanar distance d^*_{hkl} (Williamson–Hall plot). The dotted line denotes the optimized linear dependence.

4. Conclusion

We have developed an efficient and accurate algorithm to evaluate the theoretical diffraction peak profiles from spherical crystallites with lognormal size distribution. 'Lorentzian-like' or 'super-Lorentzian' line profiles are naturally predicted for broad size distributions, as has been concluded by Popa & Balzar (2002). The properties of the size distribution can be estimated by a simple curve fitting method applied to the intrinsic diffraction peak profiles from small crystallites, which can be extracted from the experimental data by the whole-pattern deconvolution method recently developed by the authors (Ida & Toraya, 2002).

APPENDIX *A*
Derivation of efficient algorithm for the numerical integral

A1. General formula

An efficient algorithm for numerical evaluation of the integral with the formula

$$S = \int_a^b f(x)g(x)\,{\rm d}x \tag{36}$$

is obtained by the substitution of the variable x by ξ, which approximates the primitive function of the integrand, *i.e.*

$$\xi \equiv H(x) \simeq \int f(x)g(x)\,{\rm d}x. \tag{37}$$

The integral is exactly evaluated by the following formula:

$$S = \int_{H(a)}^{H(b)} \{f[H^{-1}(\xi)]g[H^{-1}(\xi)]/H'[H^{-1}(\xi)]\}\,{\rm d}\xi. \tag{38}$$

When the integrand in equation (38) gradually varies with the integration variable ξ, the Gauss–Legendre quadrature, or any other numerical integral, becomes valid for the precise evaluation of the integral. Even when the function $H(x)$ is only a rough approximation for the primitive function of the integrand in equation (35), it can considerably improve the efficiency of the numerical calculation.

We assume that the functions $f(x)$ and $g(x)$ have peaks located at x_1 and x_2, respectively, and approximate formulae of the primitive functions are given by $F(x)$ and $G(x)$, *i.e.*

$$F(x) \simeq \int f(x)\,{\rm d}x \tag{39}$$

and

$$G(x) \simeq \int g(x)\,{\rm d}x. \tag{40}$$

Let us examine the following formula for $H(x)$:

$$H(x) = G[AF(x) + B]/A, \tag{41}$$

where A and B are arbitrary constants. The derivative of $H(x)$ is given by

$$\begin{aligned} H'(x) &= F'(x)G'[AF(x) + B] \\ &\simeq f(x)g[AF(x) + B]. \end{aligned} \tag{42}$$

Then, $H(x)$ will become an approximation for the primitive of $[f(x)g(x)]$ if $[AF(x) + B] \simeq x$ is satisfied. Since the value of $[f(x)g(x)]$ is significant at $x = x_1, x_2$, the following set of linear algebraic equations is assumed:

$$\begin{cases} AF(x_1) + B = x_1, \\ AF(x_2) + B = x_2, \end{cases} \tag{43}$$

the solutions of which are given by

$$A = (x_2 - x_1)/[F(x_2) - F(x_1)] \tag{44}$$

and

$$B = [x_1F(x_2) - x_2F(x_1)]/[F(x_2) - F(x_1)]. \tag{45}$$

The efficiency of the numerical integral is expected to be improved by the substitution of the variable $\xi = G[AF(x) + B]/A$, with the constants A, B given by equations (44) and (45), because it roughly satisfies the relation given by equation (37).

A2. Evaluation of synthesized peak profile

The formula of the SLN peak profile given by equation (15) can be rewritten as

$$f_{\rm SLN}(k; m, \omega) = m\exp(3.5\omega^2)\int_0^\infty [f_S(k; x)/x] \times f_{\rm LN}[x; m\exp(4\omega^2), \omega]\,{\rm d}x. \quad (46)$$

The general formula, described in the preceding section, is straightforwardly applied to the above equation for evaluating the SLN peak profile.

The function $f_{\rm LN}[x; m\exp(4\omega^2); \omega]$ has a maximum at $x_1 = m\exp(4\omega^2)$, and the exact primitive function is assigned to $F(x)$ by

$$F(x) = (1/2){\rm erfc}\{-[\ln(x/m) - 4\omega^2]/2^{1/2}\omega\}. \quad (47)$$

The function $[f_S(k; x)/x]$ has a maximum at $x_2 = 0$, and can be roughly approximated by the Lorentzian function with the same area and integral breadth,

$$G'(x) = (3/4)[1 + (3\pi kx/4)^2]^{-1}, \quad (48)$$

the primitive function of which is given by

$$G(x) = (\pi k)^{-1}\arctan(3\pi kD/4). \quad (49)$$

Then, the constants A and B are given by

$$A = 2m\exp(4\omega^2) \quad (50)$$

and

$$B = 0. \quad (51)$$

The substitution of the variable

$$\xi = G[AF(x)] \quad (52)$$

gives the following formula for the SLN profile:

$$f_{\rm SLN}(k; m, \omega) = (1/2)\exp(-0.5\omega^2)\int_\alpha^\beta g(x)/G'(y)\,{\rm d}\xi, \quad (53)$$

where

$$\alpha = G[AF(0)] = 0, \quad (54)$$

$$\beta = G[AF(\infty)] = G[2m\exp(4\omega^2)], \quad (55)$$

$$y = G^{-1}(\xi), \quad (56)$$

$$x = F^{-1}(y/A). \quad (57)$$

Note that the inverse functions of $F(x)$ and $G(x)$,

$$F^{-1}(z) = m\exp[4\omega^2 - 2^{1/2}\omega\ {\rm erfc}^{-1}(2z)] \quad (58)$$

and

$$G^{-1}(\xi) = (4/3\pi k)\tan(\pi k\xi), \quad (59)$$

are both available.

Finally, equations (25)–(33) are derived by applying the following general quadrature formulae:

$$\int_\alpha^\beta h(\xi)\,{\rm d}\xi \simeq (\beta - \alpha)\sum_{j=1}^N w_j h(\xi_j) \quad (60)$$

and

$$\xi_j = \alpha + (\beta - \alpha)x_j, \quad (61)$$

where $\{w_j\}$ are the appropriate weights for the abscissas $\{x_j\}$ ($j = 1, \ldots, N$) ranging from 0 to 1.

APPENDIX *B*
Numerical routine for the inverse error function

A concise approximation for the inverse complementary error function ${\rm erfc}^{-1}(x)$, written in C, is presented in Fig. 12.

```
#include <math.h>

double erfcinv(double X)
{
    double Z,W,WI,F,D,Z2;

    if (X>1.0) {
        return -erfcinv(2.0-X);
    }
    Z=1.0-X;
    if (Z>0.85) {
        W=sqrt(-log(X+X*Z));
        if (W>=2.5) {
            if (W>=4.0) {
                WI=1.0/W;
                F=0.01078639*WI-0.1498384;
                F=(F*WI-0.002028152)*WI;
                D=WI-0.06888301;
                D=D*WI+0.5211733;
                D=D*WI+0.09952975;
                return W+W*(0.1851159E-3+F/D);
            } else {
                F=0.06208963*W-0.3166501;
                F=(F*W+0.3937021)*W;
                D=W-2.962883;
                D=D*W+4.666263;
                D=D*W-6.266786;
                return W+W*(-0.05668422+F/D);
            }
        } else {
            F=0.05073975*W-0.2368201;
            F=(F*W-0.1314774)*W;
            D=(W-7.586103)*W+21.98546;
            D=D*W-44.27977;
            return W+W*(-0.1146666+F/D);
        }
    } else {
        Z2=Z*Z;
        F=-1.187515+Z2;
        F=-2.374996+Z2-0.05496261/F;
        F=-3.293474+Z2-1.896513/F;
        F=-0.1137730-0.5751703*Z2/F;
        return Z+Z*F;
    }
}
```

Figure 12
Concise approximation for the inverse complementary error function.

The authors are grateful for the financial support of Nippon Sheet Glass Foundation for Materials Science and Engineering.

References

Guinier, A. (1963). *X-ray Diffraction.* San Francisco: Freeman.
Ida, T. (1998*a*). *Rev. Sci. Instrum.* **69**, 2268–2272.
Ida, T. (1998*b*). *Rev. Sci. Instrum.* **69**, 3837–3839.
Ida, T. & Kimura, K. (1999*a*). *J. Appl. Cryst.* **32**, 634–640.
Ida, T. & Kimura, K. (1999*b*). *J. Appl. Cryst.* **32**, 982–991.
Ida, T. & Toraya, H. (2002). *J. Appl. Cryst.* **35**, 58–68.
Langford, J. I., Louër, D. & Scardi, P. (2000). *J. Appl. Cryst.* **33**, 964–974.

Langford, J. I. & Wilson, A. J. C. (1978). *J. Appl. Cryst.* **11**, 102–113.
Paterson, M. S. (1952). *J. Appl. Phys.* **23**, 805–811.
Plévert, J. & Louër, D. (1990). *J. Chim. Phys.* **87**, 1427–1440.
Popa, N. C. & Balzar, D. (2002). *J. Appl. Cryst.* **35**, 338–346.
Press, W. H., Flannery, B. P., Teukolsky, S. A. & Vetterling, W. T. (1986). *Numerical Recipes*. Cambridge University Press.
Stokes, A. R. (1948). *Proc. Phys. Soc. London*, **61**, 382–393.
Ungár, T., Gubicza, J., Ribárik, G. & Borbély, A. (2001). *J. Appl. Cryst.* **34**, 298–310.
Warren, B. E. & Averbach, B. L. (1950). *J. Appl. Phys.* **21**, 595–599.
Wertheim, G. K., Butler, M. A., West, K. W. & Buchanan, D. N. E. (1974). *Rev. Sci. Instrum.* **11**, 1369–1371.
Williamson, G. K. & Hall, W. H. (1953). *Acta Metall.* **1**, 22–31.